OPEN ACCESS

remote sensing

Article

Semi-Empirical Calibration of the Integral Equation Model for Co-Polarized L-Band Backscattering

Nicolas Baghdadi [1,*], Mehrez Zribi [2], Simonetta Paloscia [3], Niko E. C. Verhoest [4], Hans Lievens [4], Frederic Baup [2] and Francesco Mattia [5]

[1] IRSTEA, UMR TETIS, 500 rue François Breton, F-34093 Montpellier cedex 5, France
[2] CESBIO, 18 av. Edouard Belin, bpi 2801, 31401Toulouse cedex 9, France;
    E-Mails: mehrez.zribi@ird.fr (M.Z.); frederic.baup@cesbio.cnes.fr (F.B.)
[3] CNR-IFAC, via Madonna del Piano 10, 50019 Sesto Fiorentino, Firenze, Italy;
    E-Mail: s.paloscia@ifac.cnr.it
[4] Laboratory of Hydrology and Water Management, Ghent University, Ghent B-9000, Belgium;
    E-Mails: Niko.Verhoest@UGent.be (N.E.C.V.); Hans.Lievens@UGent.be (H.L.)
[5] CNR-ISSIA, via Amendola 122/D, Bari 70126, Italy; E-Mail: mattia@ba.issia.cnr.it

* Author to whom correspondence should be addressed; E-Mail: nicolas.baghdadi@teledetection.fr;
    Tel.: +33-467-548-724; Fax: +33-467-548-700.

Abstract: The objective of this paper is to extend the semi-empirical calibration of the backscattering Integral Equation Model (IEM) initially proposed for Synthetic Aperture Radar (SAR) data at C- and X-bands to SAR data at L-band. A large dataset of radar signal and *in situ* measurements (soil moisture and surface roughness) over bare soil surfaces were used. This dataset was collected over numerous agricultural study sites in France, Luxembourg, Belgium, Germany and Italy using various SAR sensors (AIRSAR, SIR-C, JERS-1, PALSAR-1, ESAR). Results showed slightly better simulations with exponential autocorrelation function than with Gaussian function and with HH than with VV. Using the exponential autocorrelation function, the mean difference between experimental data and Integral Equation Model (IEM) simulations is +0.4 dB in HH and −1.2 dB in VV with a Root Mean Square Error (RMSE) about 3.5 dB. In order to improve the modeling results of the IEM for a better use in the inversion of SAR data, a semi-empirical calibration of the IEM was performed at L-band in replacing the correlation length derived from field experiments by a fitting parameter. Better agreement was observed between the backscattering coefficient

provided by the SAR and that simulated by the calibrated version of the IEM (RMSE about 2.2 dB).

Keywords: integral equation model; synthetic aperture radar; L-band; bare soil

1. Introduction

Soil moisture content and roughness play an important role in hydrology. These soil parameters could be estimated using Synthetic Aperture Radar (SAR) irrespective of the meteorological conditions. However, these estimations require the use of a radar backscattering model that is capable of correctly modeling the radar signal. The Integral Equation Model (IEM) [1,2] is widely used in inversion procedures of SAR images for retrieving soil moisture content and roughness (e.g., [3–9]). Its validity domain covers the range of surface roughness values (root mean square height "*rms*") encountered on agricultural soils ($k.rms \leq 3$, where k is the wave number $= 0.24$ cm^{-1} for a frequency in L-band of 1.25 GHz).

The IEM simulates the radar backscattering coefficient (σ°) for bare soils given sensor parameters (radar wavelength, incidence angle, and polarization) and soil characteristics (dielectric constant, standard deviation of heights, correlation length, and autocorrelation function "ACF"). Most studies reported discrepancies between modeled backscatters by IEM and observed backscatters by SAR sensors at L-, C-, and X-bands [10–20]. These discrepancies could be related to the inaccuracy of the roughness measurements, which introduces significant errors into the modeled radar signal [21,22], and to the model itself [10–15]. Indeed, according to Lievens *et al.* [21] and Oh and Kay [22], correlation length measurements are unreliable when short roughness profiles are used or when the number of profiles is limited (error over 50%). Thus, the estimation of soil parameters (moisture content and roughness) from SAR images can be inaccurate using such a model.

Baghdadi *et al.* [10–14] proposed a semi-empirical calibration of the IEM at C- and X-bands, based on experimental data of SAR images and ground measurements (soil moisture content and roughness). The calibration consisted of finding a fitting parameter which replaces the correlation length measurement so that the IEM reproduces better the radar backscattering coefficient. Calibration results showed that the fitting parameter was found dependent on *rms* surface height, radar wavelength, polarization, and incidence angle. Given the successful application at C- and X-bands, this paper aims at deriving similar equations for L-band.

The first objective of this study is to evaluate the IEM using dataset acquired over numerous study sites in Europe (France, Luxembourg, Belgium, Germany and Italy). Simulated backscattering coefficients from the IEM will be compared to the backscattered signal registered by several SAR systems at L-band and HH and VV polarizations (AIRSAR, SIR-C, JERS-1, PALSAR-1, ESAR). Next, a semi-empirical calibration of the IEM is proposed as was already derived by previous studies for C- and X-bands SAR data in order to improve the modeling of the radar signal by the IEM. Section 2 describes the dataset. In Section 3, a comparison between modeled and observed backscatters is presented. The semi-empirical calibration methodology of the IEM is proposed in Section 4 and its performance evaluated in Section 5. A summary of the results is provided in the last Section 6.

2. Dataset Description

Experimental dataset of SAR images and measurements of soil moisture content and roughness acquired over bare soils were used. This dataset was collected over numerous agricultural study sites in France (2 sites), Luxembourg (1 site), Belgium (2 sites), Germany (1 site), and Italy (2 sites) (Figure 1, Table 1).
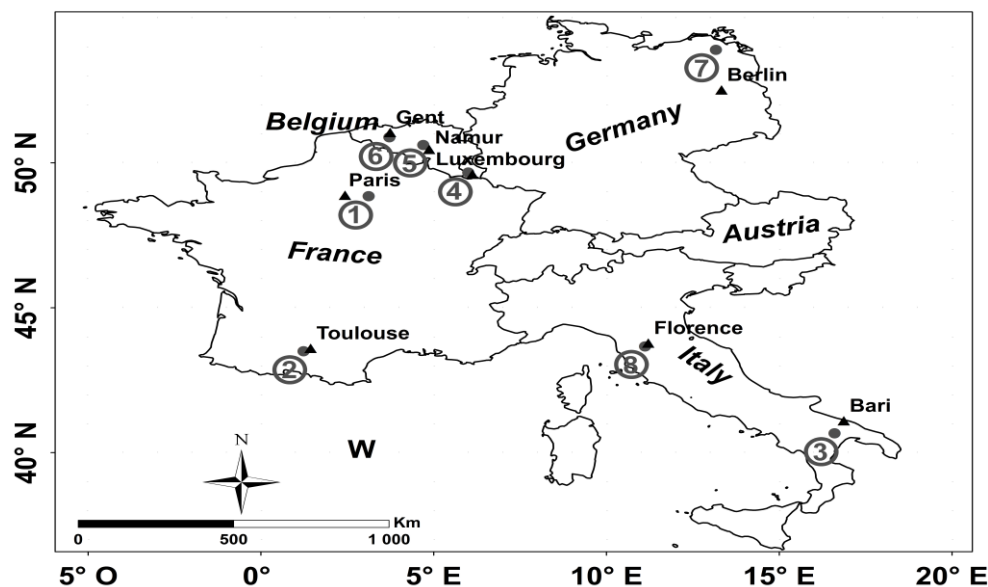
Figure 1. Location of various study sites. "1": Orgeval; "2": Saint Lys; "3": Matera; "4": Alzette; "5": Dijle; "6": Zwalm; "7": Demmin; "8": Montespertoli.

SAR images were acquired by various airborne and spaceborne sensors (AIRSAR, SIR-C, JERS-1, PALSAR-1, ESAR) operating at L-band (~1.25 to 1.30 GHz), with incidence angles between 21.5 °and 57 °, and in HH and VV polarizations. For experimental bare soil plots, the mean backscattering coefficients are calculated from calibrated SAR images by linearly averaging the σ °values of all pixels within the plot. Only plots with a homogeneous surface (similar soil type, moisture content and surface roughness) of around one hectare or more (about 100 pixels for SAR images with a spatial resolution of 10 m × 10 m) were used (which helps reducing speckle). In addition, *in situ* ground measurements of soil moisture content (*mv*) and roughness were carried out for each experimental plot. The soil moisture measurements were collected from the top 5 or 10 cm of each experimental plot using the gravimetric method or/and a calibrated TDR (Time Domain Reflectometry) probe. For wet soil conditions, the soil moisture measurements were collected from the top 5 cm and from the top 10 cm for dry soil conditions. Nolan and Fatland [23] found that in a clay loam soil, the penetration depth of L-band radar signals decreased from approximately 10 cm in the case of 5 vol % soil moisture content, to 5 cm when the soil moisture content increased to 15 vol %. In practice, the soil moisture for each experimental plot is assumed to be equal to the mean value measured from several samples (the number of soil moisture samples depends on the size of experimental plots). The single-field standard deviation of soil moisture is lower than 2 vol % for 95% of the measurements.

Table 1. Main characteristics of the dataset used in this study.

Site	Lat/Long	Texture Composition (Silt; Clay; Sand)	SAR Sensor	Pixel Spacing (m ×m)	Freq (GHz)	Year	Number of Data for Each SAR Configuration
Orgeval (Fr) [24]	48 °51′ N 3 °07′ E	(78%; 17%; 5%)	SIR-C	12.5 × 12.5	1.25	1994	HH: 52 °(5), 55 °(5), 57 °(5) VV: 52 °(5), 55 °(5), 57 °(5)
Orgeval (Fr)	48 °51′ N 3 °07′ E	(78%; 17%; 5%)	PALSAR-1	12.5 × 12.5	1.27	2009	HH: 21.5 °(7) VV: 21.5 °(7)
Saint Lys (Fr) [25]	43 °30′ N 01 °14′ E	(50%; 16%; 34%)	PALSAR-1	6.25 × 6.25 12.5 × 12.5	1.27	2010	HH: 38.7 °(15)
Matera (It) [17]	40 °40′ N 16 °36′ E	(59%; 14%; 27%)	SIR-C	12.5 × 12.5	1.25	1994	HH: 45.8 °(6) VV: 45.8 °(6)
Alzette (Lu) [26]	49 °40′ N 06 °00′ E	(50%; 30%; 20%)	PALSAR-1	12.5 × 12.5	1.27	2008	HH: 36.5 °–41.1 °(4)
Dijle (Be) [26]	50 °37′ N 04 °42′ E	(84%; 12%; 4%)	PALSAR-1	12.5 × 12.5	1.27	2008; 2009	HH: 36.2 °–39.4 °(12)
Zwalm (Be) [26]	50 °53′ N 03 °43′ E	(72%; 13%; 15%)	PALSAR-1	12.5 × 12.5	1.27	2007	HH: 38.7 °(2)
Demmin (Ge) [26]	53 °54′ N 13 °10′ E	(25%; 7%; 68%)	ESAR	2 ×2	1.30	2006	HH: 40 °–48.4 °(9)
Montespertoli (It) [27]	43 °40′ N 11 °7′ E	(40%; 20%; 40%)	AIRSAR	12.5 × 12.5	1.26	1991	HH: 25 °(7), 35 °(7), 50 °(7) VV: 25 °(7), 35 °(7), 50 °(7)
Montespertoli (It) [28]	43 °40′ N 11 °7′ E	(40%; 20%; 40%)	SIR-C	12.5 × 12.5	1.25	1994	HH: 25 °(25), 35 °(8), 45 °(22) VV: 25 °(25), 35 °(8), 45 °(8)
Montespertoli (It) [29]	43 °40′ N 11 °7′ E	(40%; 20%; 40%)	JERS-1	12.5 × 12.5	1.27	1994	HH: 35 °(8)

Roughness measurements are made using laser or needle profilometers (1, 2 and 3 m long and with 0.5, 1, 1.5, and 2 cm sampling intervals) and meshboard (4 m long) with several roughness profiles for each experimental plot, parallel and perpendicular to tillage direction. From these roughness measurements, the root mean square (*rms*) surface height and the correlation length (*L*) are calculated using the mean of all ACFs.

The *in situ* measurements accuracy of *rms* and *L* depends on the roughness profile length and sampling interval (e.g., [21,22,30]). In our database, the roughness parameter *rms* has been estimated with an accuracy ranging between 5% and 10%, and the *L*-values with an accuracy ranging between 10% and 20% [20,21]. Low uncertainties on the roughness parameters measurements are obtained for high length and low sampling interval of the roughness profiles.

Soil moisture, *rms* surface height, and correlation length range respectively from 3.5 to 40.9 vol %, 0.65 to 9.55 cm, and from 2.37 to 38.50 cm. A total of 154 experimental data points is available in HH and 90 in VV.

3. Evaluation of the IEM

The Integral Equation Model (IEM) developed by Fung *et al.* [1] is a theoretical radar backscattering model that is widely used for soil moisture content and roughness estimation. At L-band, the IEM has a validity domain that covers the range of roughness values that are commonly encountered for agricultural surfaces. The IEM simulates the radar backscattering coefficient from the radar wavelength, the incidence angle, the polarization, the soil *rms* surface height, the soil correlation length, the ACF, and the soil dielectric constant derived from the moisture content and the soil texture [31]. Over bare soils in agricultural areas, the ACF is exponential for low soil roughness values and Gaussian for high soil roughness values [2].

Table 2. Statistics for the evaluation of Integral Equation Model (IEM). Bias = SAR–IEM; MAE = Mean Absolute Error; RMSE = Root Mean Square Error.

Polarization	Autocorrelation Function	Bias (dB)	MAE (dB)	RMSE (dB)
HH	Exponential; all *rms* values	+0.4	2.5	3.2
	Exponential; *rms* < 3 cm	+0.6	2.2	2.9
	Exponential; *rms* > 3 cm	−0.3	3.2	3.9
HH	Gaussian; all *rms* values	−1.2	2.9	3.8
	Gaussian; *rms* < 3 cm	−0.5	2.7	3.9
	Gaussian; *rms* > 3 cm	−2.7	3.1	3.7
VV	Exponential; all *rms* values	−1.2	3.0	3.7
	Exponential; *rms* < 3 cm	−2.2	2.9	3.5
	Exponential; *rms* > 3 cm	+1.6	3.5	4.1
VV	Gaussian; all *rms* values	−2.5	3.9	5.0
	Gaussian; *rms* < 3 cm	−2.8	4.4	5.6
	Gaussian; *rms* > 3 cm	−1.8	2.5	3.2

Comparison between the IEM simulations and the experimental dataset was done for both exponential and Gaussian ACFs (Table 2, Figure 2). Simulation results were slightly better with the exponential ACF than with the Gaussian ACF. Similarly, HH provides slightly better results than VV. With the

exponential ACF, the mean difference between experimental data and IEM simulations is +0.4 dB in HH and −1.2 dB in VV with an RMSE about 3.5 dB (3.2 in HH and 3.7 dB in VV). The use of Gaussian ACF causes higher biases in comparison to the exponential ACF (−1.2 dB in HH and −2.5 dB in VV), and RMSE of the same order of magnitude in HH (3.8 dB) but higher in VV (5.0 dB). Other studies have reported a tendency of the IEM to overestimate observed L-band backscatter values [16,17].
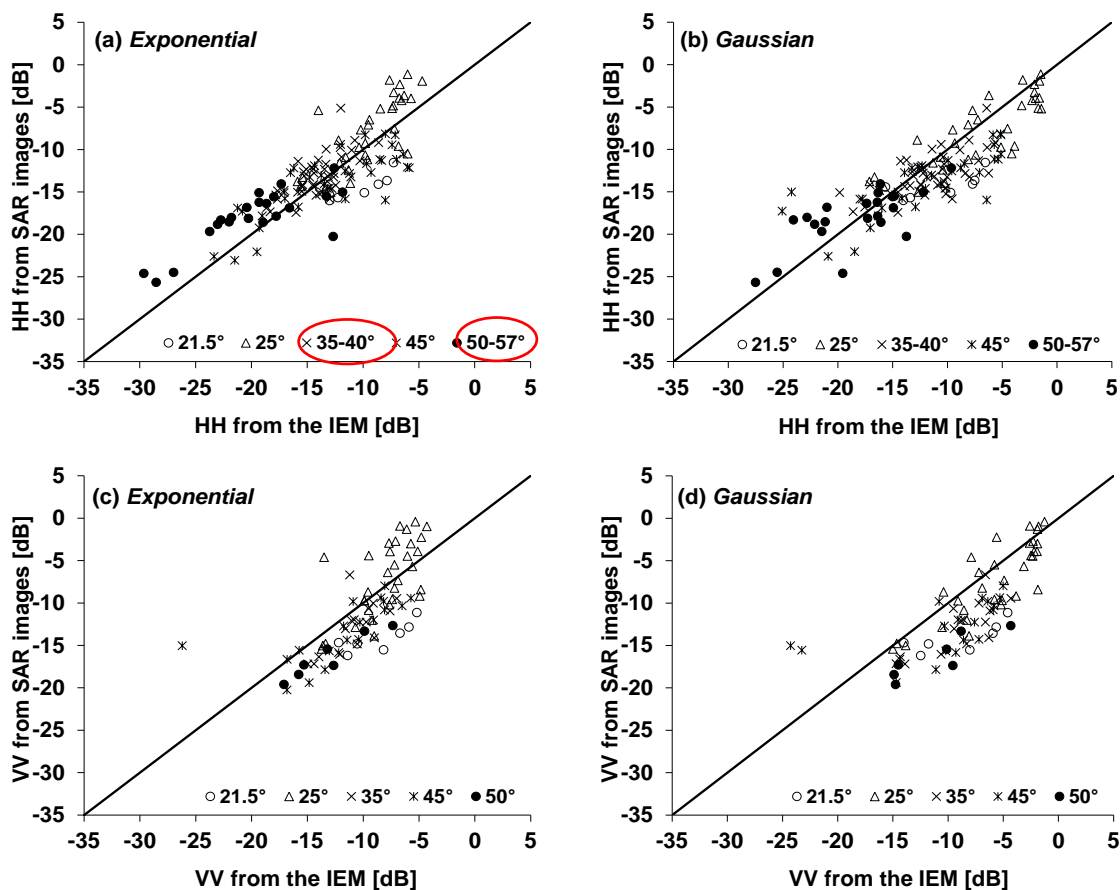
Figure 2. Observed backscatter coefficients from Synthetic Aperture Radar (SAR) images (L-band) *vs.* modeled backscatter values from IEM (at different incidence angles) using correlation length measurements, for exponential and Gaussian autocorrelation function (ACFs). Mean of the difference between SAR and IEM and root mean square error were calculated for all *rms* values. (**a**): HH polarization and exponential ACF, (**b**): HH polarization and Gaussian ACF, (**c**): VV polarization and exponential ACF, (**d**): VV polarization and Gaussian ACF.

Many studies used for validation the IEM show an even more limited validity domain $k.rms < 1$ [24,32] than the one defined initially by Fung *et al.* [1,2] $k.rms < 3$. Consequently, the error in the modeling of radar backscattering coefficients was also analyzed as a function of *rms* surface height classes (*rms* < 3 cm and *rms* > 3 cm, corresponding to $k.rms < 1$). Results showed that the exponential ACF provides better IEM simulations for values of *rms* lower than 3 cm (RMSE = 2.9 dB for HH and 3.5 dB for VV with the exponential ACF, and RMSE = 3.9 dB for HH and 5.6 dB for VV with the Gaussian ACF) (Table 2). For values of *rms* greater than 3 cm, the use of Gaussian ACF is more relevant (RMSE = 3.7

dB for HH and 3.2 dB for VV with the Gaussian ACF, and RMSE = 3.9 dB for HH and 4.1 dB for VV with the exponential ACF) (Table 2).

4. IEM Semi Empirical Calibration Methodology

The description of surface roughness in the IEM is based on three parameters: the *rms* surface height, the correlation length, and the ACF. As the modeled backscattering coefficient depends on the shape of the ACF chosen, the use of the IEM in operational mode for estimating the soil moisture content from SAR images, at a given spatial scale (sub-plot, plot, *etc.*), requires knowledge on the ACF shape which depends on the *rms* surface height value (generally exponential for smooth surfaces and Gaussian for rough surfaces). As the *rms* values are also unknown during model inversion, it is therefore difficult to choose the required ACF, which therefore would lead to an inaccurate retrieval of the soil moisture. In fact, the use of the unsuitable autocorrelation function leads to important errors on the backscattering coefficients estimation. For *rms* lower than 3 cm, the use of Gaussian ACF instead of an exponential ACF leads to an error increase up to 2.1 dB on the retrieval of backscattering coefficients (Table 2).

For *rms* greater than 3 cm, the use of exponential ACF instead of Gaussian ACF leads to an error increase up to 0.9 dB (Table 2). Consequently, an additional uncertainty on the retrieval of backscattering coefficients of only 1 dB may lead to additional uncertainty on the soil moisture estimates by about 5 vol % for sensitivity of radar signal in L-band of 0.2 dB for 1 vol % [33].

Moreover, the measurements of correlation length are often the less accurate in comparison to other measured soil parameters [21,22], and the discrepancies noted between IEM simulations and SAR data could be attributed to the uncertainty of the correlation length measurements and to the model itself [10,13–15]. Thus, the semi empirical calibration of the IEM consisted in the replacement of the experimental correlation length by a fitting parameter in order to ensure better matching between simulations and SAR data [10,13,14]. In Baghdadi *et al.* [10,13,14], the calibration parameter was found to be dependent on surface roughness, incidence angle, polarization, and radar wavelength. In addition, with this Baghdadi calibration method, bare soils will be characterized by two surface parameters (*rms* surface height and moisture content) instead of three (*rms* surface height, correlation length and moisture content), in case the ACF is predefined for the entire range of *rms* surface heights.

Given the robustness of the IEM semi-empirical calibration proposed in Baghdadi *et al.* [10,14] for C- and X-bands SAR data as demonstrated in (e.g., [16,18,20]), the objective is to extend the same approach to L-band in order to improve the SAR backscatter prediction. The prediction error on the radar backscattering coefficients based on a 10-fold cross-validation was estimated for each polarization in order to validate the predictive performance of the calibrated version of the IEM (dataset was randomly divided into 90% training and 10% validation data elements and this procedure was repeated 10 times).

The method consists of replacing for each training data element the experimental correlation length by a fitting parameter (*Lopt*) which ensures a good fit between the backscattering coefficient provided by the SAR sensor and that simulated by the IEM. This approach considers the same correlation function irrespective to the range of *rms* surface height.

5. Results and Discussion

Figure 3 shows the behavior of the IEM as a function of the correlation length, for the exponential and Gaussian ACFs. As illustrated, *Lopt* has two possible solutions, *Lopt1* (the lowest value) and *Lopt2* (the highest value). Results showed that *Lopt1* values in HH were higher than those in VV for both exponential and Gaussian ACFs, whereas *Lopt2* values were similar in HH and VV for both ACFs. Increasing of IEM in the first part of simulations corresponds to very short correlation lengths. For these short *Lopt*-values, the IEM is out of its validity domain [1] (Figure 4). Only the second part, with a decrease of the radar signal when the correlation length increases, corresponds to IEM validity domain (Figure 4). Thus, only *Lopt2* can be retained. In addition, when we consider realistic correlation lengths for agricultural soils (approximately higher than 3 cm), we observe a decreasing of radar signal in L, C and X bands as the correlation length increases. However, for lower frequencies, like P band, we observe clearly an increasing of radar signal function of correlation length.
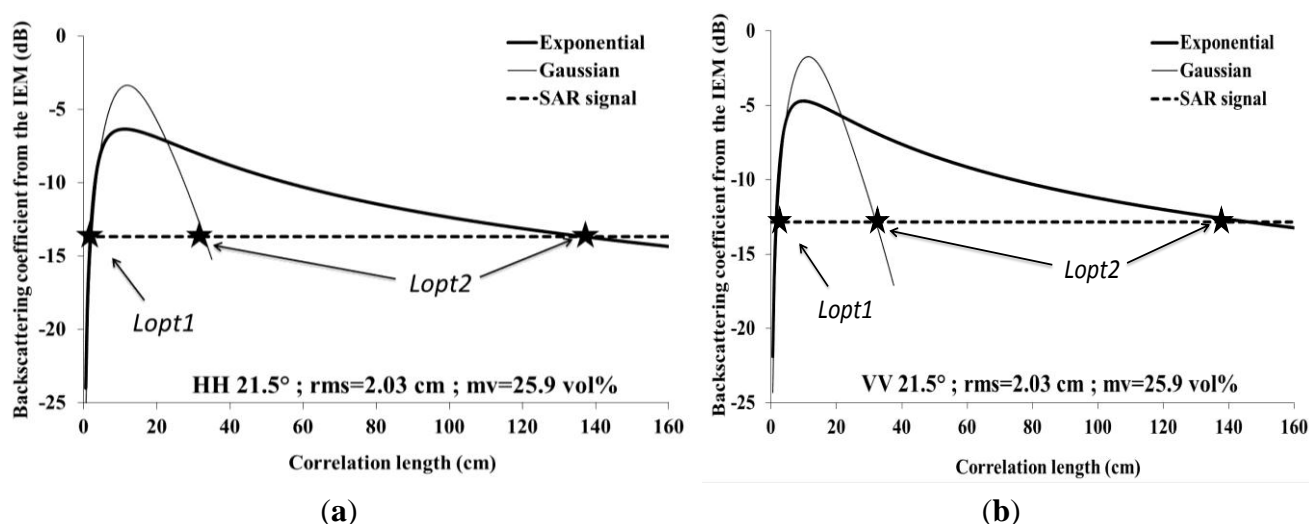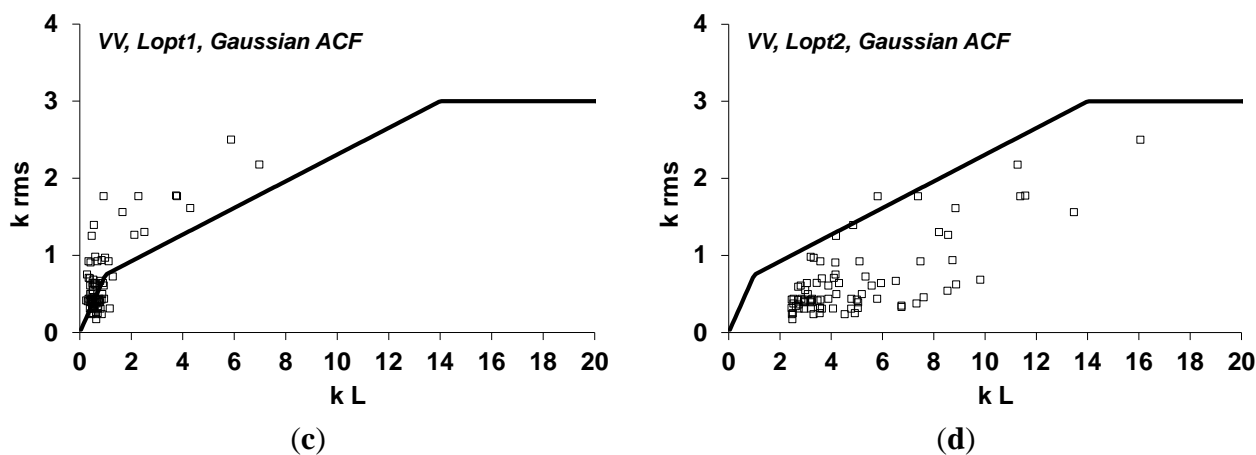

Figure 3. Behaviour of the IEM as a function of correlation length for a given plot, with Gaussian and exponential ACFs. (**a**): HH polarization, (**b**): VV polarization.
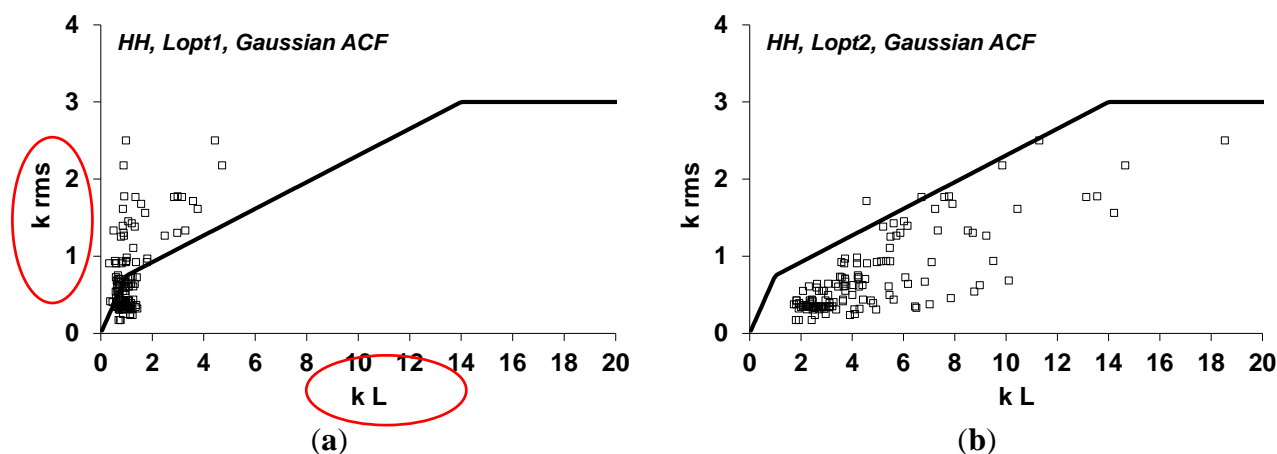
Figure 4. *Cont.*

Figure 4. Validity regions of the IEM model in *k.rms - L* space (where *k* is the wave number) for Gaussian ACF, and the location of experimental data points [1]. All experimental data points are within the IEM limits with *Lopt2*. (**a**): HH polarization and *L=Lopt1*, (**b**): HH polarization and *L=Lopt2*, (**c**): VV polarization and *L=Lopt1*, (**d**): VV polarization and *L=Lopt2*.

For each dataset element, the fitting procedure has a higher probability to find an estimation of *Lopt2* for the Gaussian ACF than for the exponential ACF since the $\sigma°$ simulated from the IEM has a higher amplitude for the Gaussian ACF (Figure 3). Therefore, the probability of intersecting the SAR signal with the IEM response is higher for the Gaussian ACF. Thus, our set of *Lopt2* data, calculated for each polarization, is consequently larger with the Gaussian ACF which justifies its use to fit the best regressions between *Lopt2* and *rms* height as a function of incidence angle and polarization. A linear relationship between *Lopt2* with the Gaussian ACF and *rms* ($\alpha + \beta$ *rms*; α and β are dependent on polarization and incidence angle "θ") ensures a correct modeling of the physical behavior of the IEM ($\sigma°$ increases with *rms* surface height for the whole range of *rms*-values):

$$Lopt2\,(rms, \theta, HH) = 2.6590\,\theta^{-1.4493} + 3.0484\,rms\,\theta^{-0.8044} \tag{1}$$

$$Lopt2\,(rms, \theta, VV) = 5.8735\,\theta^{-1.0814} + 1.3015\,rms\,\theta^{-1.4498} \tag{2}$$

θ is in radian, *Lopt2* and *rms* are in cm. The coefficients given in Equations (1) and (2) were derived using the entire dataset. However, during the cross-validation, coefficients were calculated using the associated training dataset.

For subsequent applications, *Lopt2* obtained with the Gaussian ACF (Equations (1) and (2)) replaces the experimental correlation length in the IEM.

Figure 5 shows the fitting parameter *Lopt2* obtained with the Gaussian ACF. Results showed that the fitting parameter *Lopt2* is strongly dependent on *rms* surface height and the incidence angle. It increases as the *rms* increases and decreases with the incidence angle (Figure 5). The dependence between *Lopt2* and the incidence angle becomes weak for $\theta > 35°$. In addition, Figure 6a shows that the fitting parameter *Lopt2* is higher than the experimental correlation length and that *Lopt2* is similar for HH and VV polarizations. The experimental correlation length also showed an increase with the *rms* surface height (Figure 6b).
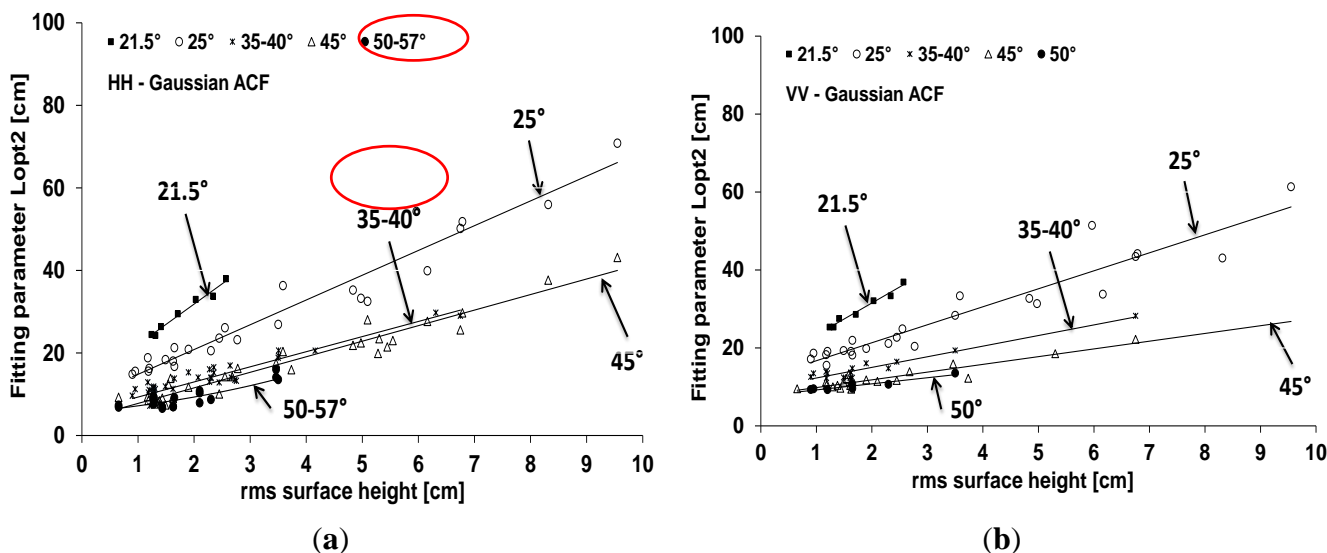
Figure 5. Fitting parameter *Lopt2* as a function rms surface height with the Gaussian ACF. (**a**): HH polarization, (**b**) VV polarization.
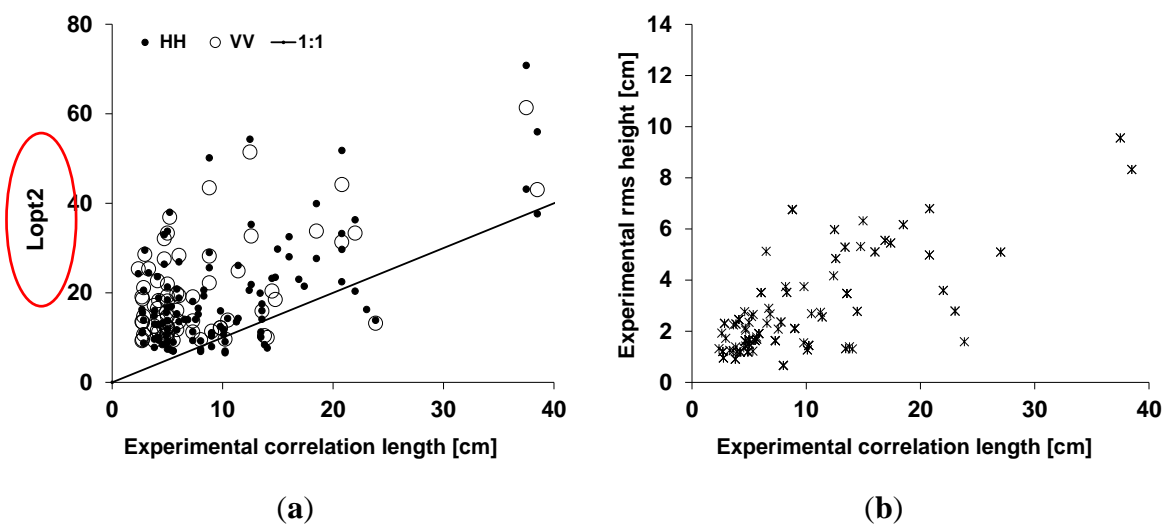

Figure 6. Relationship between (**a**) *Lopt2* with Gaussian ACF and the experimental correlation length; (**b**) the root mean square surface height and the experimental correlation length obtained from *in situ* measurements.

The effect of the radar frequency on the IEM calibration was done by comparing the expressions of *Lopt2* obtained by Baghdadi *et al.* [12,14] and Zribi and Baghdadi [34] at C- and X-bands to those obtained in this study for L-band (Figure 7). Results showed that *Lopt2* increases as the radar wavelength increases.
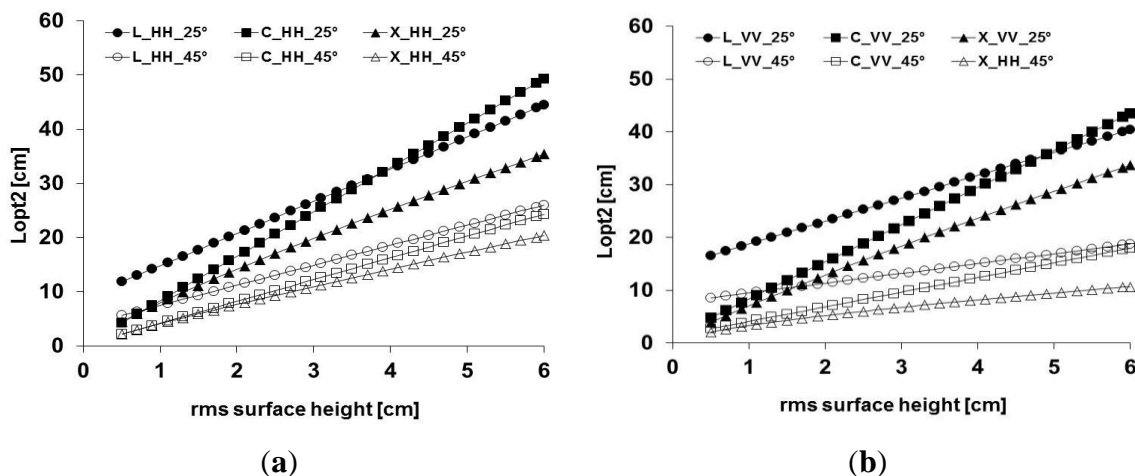
Figure 7. Comparison between *Lopt2* obtained in this study for L-band and those obtained in previous studies for C- and X-bands [12,14,34]. Gaussian ACF was used. (**a**) HH; (**b**) VV.

Finally, to validate the generalization performance of *Lopt2* (Equations (1) and (2)), a 10-fold cross validation was used. The error in the modeling of radar backscattering coefficients by the calibrated version of the IEM was assessed. Results showed that the proposed semi-empirical calibration of the IEM provides improved results (Figure 8 in comparison to Figure 2 and Table 2). The biases and the RMSE have decreased for both HH and VV polarizations. The RMSE decreased from 3.2 dB with the exponential ACF and 3.8 dB with the Gaussian ACF to 2.2 dB for HH, and from 3.7 dB with the exponential ACF and 5.0 dB with the Gaussian ACF to 2.3 dB for VV (Table 2, Figure 8). We observe a small mean difference between SAR data and calibrated IEM simulations for both polarizations (less than 0.5 dB). In addition, the mean absolute error (MAE) was significantly reduced in using the fitting parameter *Lopt2* (Table 2; Figure 8). The cross-validation was also considered by changing the percentages of training and validation datasets: 90% for training and 10% for validation, 80% for training and 20% for validation, and finally 50% for training and 50% for validation). The results obtained on the prediction error of the radar backscattering were similar (difference lower than 0.2 dB).
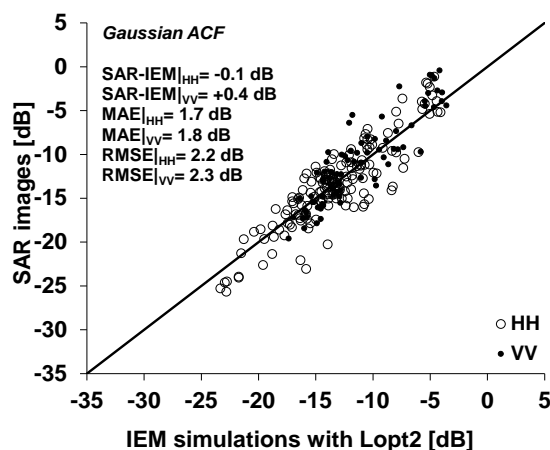
Figure 8. Validation of the semi-empirical calibration approach in using the fitting parameter *Lopt2*. Mean of the difference between SAR and IEM and root mean square error were calculated.

In order to demonstrate the calibration method relevance on study sites that were not used in the calibration dataset, we then made a k-fold cross validation where k is the number of study sites (*k* = 11 for HH polarization and *k* = 5 for VV polarization). For each of k study sites, (*k* - 1) folds were used for training and the remaining one for testing. The advantage of this k-fold cross validation is that all the study sites in the dataset are used for both training and testing. Results showed similar results with an RMSE on the backscattering coefficient estimates of 2.2 dB for HH and 2.4 for VV.

6. Conclusions

The Integral Equation Model (IEM) was evaluated using L-band SAR data (HH and VV polarizations, incidence angles between 21.5 ° and 57 °) together with *in situ* measurements (soil moisture and surface roughness) on bare soils in agricultural environments. A large dataset collected over numerous agricultural study sites in France, Luxembourg, Belgium, Germany and Italy using various SAR sensors (AIRSAR, SIR-C, JERS-1, PALSAR-1, ESAR) were used.

Simulation results were slightly better with exponential autocorrelation function than with Gaussian function. Similarly, HH provides slightly better results than VV. With the exponential function, the mean difference between SAR data and IEM simulations reaches −1.2 dB in VV with an RMSE of 3.7 dB. Simulations performed with the Gaussian function show biases of −1.2 dB in HH and −2.5 dB in VV, and RMSE of 3.8 dB in HH and 5.0 dB in VV.

A semi-empirical calibration of the IEM was proposed in order to improve the fitting of the IEM simulations to SAR response in HH and VV polarizations. Similar to approaches for C- and X-bands, the dependence of the fitting parameter on *rms* surface height, incidence angle, polarization, and radar wavelength is found for L-band. With this calibration, agricultural bare soils can be characterized by only two surface parameters (*rms* height and soil moisture) instead of four (*rms* height, correlation length, autocorrelation function, and soil moisture) since the soil correlation length is replaced by a fitting parameter for a Gaussian ACF. Results showed that this calibration ensures better agreement between IEM and the SAR data and increases the model's applicability (an improvement which can reach 3 dB for RMSE and 2 dB for MAE). Indeed, the decrease in error on the modeling of the SAR signal of about 1 dB will allow for improving the soil moisture estimates at least 3 vol % if we consider the sensitivity of the radar signal to soil moisture of about 0.3 dB/vol % [35].

Author Contributions

Conflicts of Interest

The authors declare no conflict of interest.

References

1. Fung, A.K.; Li, Z.; Chen, K.S. Backscattering from a randomly rough dielectric surface. *IEEE Trans. Geosci. Remote Sens.* **1992**, *30*, 356–369.
2. Fung, A.K. *Microwave Scattering and Emission Models and Their Applications*; Artech House, Inc.: Boston, MA, USA; London, UK, 1994; p. 573.
3. Baghdadi, N.; Gaultier, S.; King, C. Retrieving surface roughness and soil moisture from SAR data using neural network. *Can. J. Remote Sens.* **2002**, *28*, 701–711.
4. Jiancheng, S.; Chen, K.S.; Qin, L.; Jackson, T.J.; O'Neill, P.E.; Leung, T. A parameterized surface reflectivity model and estimation of bare-surface soil moisture with L-band radiometer. *IEEE Trans. Geosci. Remote Sens.* **2002**, *40*, 2674–2686.
5. Zribi, M.; Baghdadi, N.; Guérin, C. Analysis of surface roughness heterogeneity and scattering behaviour for radar measurements. *IEEE Trans. Geosci. Remote Sens.* **2006**, *44*, 2438–2444.
6. Le Morvan, A.; Zribi, M.; Baghdadi, N.; Chanzy, A. Soil moisture profile effect on radar signal measurement. *Sensors* **2008**, *8*, 256–270.
7. Baghdadi, N.; Cresson, R.; el Hajj, M.; Ludwig, R.; la Jeunesse, I. Estimation of soil parameters over bare agriculture areas from C-band polarimetric SAR data using neural networks. *Hydrol. Earth Syst. Sci.* (*HESS*) **2012**, *16*, 1607–1621.
8. He, B.; Xing, M.; Bai, X. A synergistic methodology for soil moisture estimation in an Alpine prairie using radar and optical satellite data. *Remote Sens.* **2014**, *6*, 10966–10985.
9. McNairn, H.; Merzouki, A.; Pacheco, A.; Fitzmaurice, J. Monitoring Soil Moisture to Support Risk Reduction for the Agriculture Sector Using RADARSAT-2. *IEEE J. Sel. Top. Appl. Earth Obs. Remote Sens.* **2012**, *5*, 824–834.
10. Baghdadi, N.; King, C.; Chanzy, A.; Vigneron, J.P. An empirical calibration of IEM model based on SAR data and measurements of soil moisture and surface roughness over bare soils. *Int. J. Remote Sens.* **2002**, *23*, 4325–4340.
11. Baghdadi, N.; Gherboudj, I.; Zribi, M.; Sahebi, M.; Bonn, F.; King, C. Semi-empirical calibration of the IEM backscattering model using radar images and moisture and roughness field measurements. *Int. J. Remote Sens.* **2004**, *25*, 3593–3623.
12. Baghdadi, N.; Holah, N.; Zribi, M. Calibration of the Integral Equation Model for SAR data in C-band and HH and VV polarizations. *Int. J. Remote Sens.* **2006**, *27*, 805–816.

13. Baghdadi, N.; Abou Chaaya, J.; Zribi, M. Semi-empirical calibration of the Integral equation Model for SAR data in C-band and cross polarization using radar images and field measurements. *IEEE Geosci. Remote Sens. Lett.* **2011**, *8*, 14–18.

14. Baghdadi, N.; Saba, E.; Aubert, M.; Zribi, M.; Baup, F. Comparison between backscattered TerraSAR signals and simulations from the radar backscattering models IEM, Oh, and Dubois. *IEEE Geosci. Remote Sens. Lett.* **2011**, *8*, 1160–1164.

15. Baghdadi, N.; Zribi, M. Evaluation of radar backscatter models IEM, Oh and Dubois using experimental observations. *Int. J. Remote Sens.* **2006**, *27*, 3831–3852.

16. Panciera, R.; Tanase, M.A.; Lowell, K.; Walker, J.P. Evaluation of IEM, Dubois, and Oh radar backscatter models using airborne L-band SAR. *IEEE Trans. Geosci. Remote Sens.* **2014**, *52*, 4966–4979.

17. Mattia, M.; Toan, T.L.; Souyris, J.C.; Carolis, G.D.; Floury, N.; Posa, F.; Pasquariello, G. The effect of surface roughness on multifrequency polarimetric SAR data. *IEEE Trans. Geosci. Remote Sens.* **1997**, *35*, 954–966.

18. Merzouki, A.; McNairn, H.; Pacheco, A. Evaluation of the Dubois, Oh, and IEM radar backscatter models over agricultural fields using C-band RADARSAT-2 SAR image data. *Can. J. Remote Sens.* **2010**, 36, S274–S286.

19. Wang, J.R.; Hsu, A.; Shi, J.C; O'Neill, P.E.; Engman, E.T. A comparison of soil moisture retrieval models using SIR-C measurements over Little Washita River Watershed. *Remote Sens. Environ.* **1997**, *59*, 308–320.

20. Gorrab, A.; Zribi, M.; Baghdadi, N.; Mougenot, B.; Lili-Chabaane, Z. Potential of X-band TerraSAR-X and COSMO-SkyMed SAR data for the assessment of physical soil parameters. *Remote Sens.* **2015**, *7*, 747–766.

21. Lievens, H.; Vernieuwe, H.; Álvarez-Mozos, J.; de Baets, B.; Verhoest, N.E.C. Error in radar-derived soil moisture due to roughness parameterization: An analysis based on Synthetical surface profiles. *Sens. J.* **2009**, *9*, 1067–1093.

22. Oh, Y.; Kay, Y. Condition for precise measurement of soil surface roughness. *IEEE Trans. Geosci. Remote Sens.* **1998**, *36*, 691–695.

23. Nolan, M.; Fatland, D.R. Penetration depth as a DInSAR observable and proxy for soil moisture. *IEEE Trans. Geosci. Remote Sens.* **2003**, *41*, 532–537.

24. Zribi, M.; Taconet, O.; le Hégarat-Mascle, S.; Vidal-Madjar, D.; Emblanch, C.; Loumagne, C.; Normand, M. Backscattering behavior and simulation comparison over bare soils using SIRC/XSAR and ERASME 1994 data over Orgeval. *Remote Sens. Environ.* **1997**, *59*, 256–266.

25. Baup, F.; Fieuzal, R.; Marais-Sicre, C.; Dejoux, J.-F.; le Dantec, V.; Mordelet, P.; Claverie, M.; Hagolle, O.; Lopes, A.; Keravec, P.; *et al*. MCM'10: An experiment for satellite multi-sensors crop monitoring. From high to low resolution observations. In Proceedings of the Geoscience and Remote Sensing Symposium, Munich, Germany, 22–27 July 2012; pp. 4849–4852.

26. Lievens, H.; Verhoest, N.E.C.; de Keyser, E.; Vernieuwe, H.; Matgen, P.; Álvarez-Mozos, J.; de Baets B. Effective roughness modelling as a tool for soil moisture retrieval from C-and L-band SAR. *Hydrol. Earth Syst. Sci.* **2011**, *15*, 151–162.

27. Baronti, S.; Del Frate, F.; Ferrazzoli, P.; Paloscia, S.; Pampaloni, P.; Schiavon, G. SAR polarimetric features of agricultural areas. *Int. J. Remote Sens.* **1995**, *16*, 2639–2656.

28. Macelloni, G.; Paloscia, S.; Pampaloni, P.; Sigismondi, S.; de Matthaeis, P.; Ferrazzoli, P.; Schiavon, G.; Solimini, D. The SIR-C/X-SAR experiment on Montespertoli: Sensitivity to hydrological parameters. *Int. J. Remote Sens.* **1999**, *20*, 2597–2612.

29. Paloscia, S.; Macelloni, G.; Pampaloni, P.; Sigismondi, S. The potential of C- and L-band SAR in estimating vegetation biomass: The ERS-1 and JERS-1 Experiments. *IEEE Trans. Geosci. Remote Sens.* **1999**, *37*, 2107–2110.

30. Baghdadi, N.; Paillou, P.; Davidson, M.; Grandjean, G.; Dubois, P. Relationship between profile length and roughness parameters for natural surfaces. *Int. J. Remote Sens.* **2000**, *21*, 3375–3381.

31. Hallikaïnen, M.T.; Ulaby, F.T.; Dobson, F.T.; el Rayes, M.C.; Wu, L.K. Microwave dielectric behavior of wet soil. Part I: Empirical models and experimental observations. *IEEE Trans. Geosci. Remote Sens.* **1985**, *23*, 25–34.

32. Rakotoarivony, L.; Taconet, O.; Vadal-Madjar, D.; Benallegue, M. Radar backscattering over agricultural bare soils. *J. Electromagn. Waves Appli.* **1996**, *10*, 187–209.

33. Narvekar, P.S.; Entekhabi, D.; Kim, S.B.; Njoku, E.G. Soil Moisture Retrieval Using L-Band Radar Observations. *IEEE Trans. Geosci. Remote Sens.* **2015**, *53*, 3492–3506.

34. Zribi, M.; Baghdadi N. Potential of high spatial resolution radars for the characterization of soil properties. In *Soils and Sediments as Archives of Environmental Change. Geoarchaeology and Landscape Change in the Subtropics and Tropics*; Lucke, B., Bäumler, R., Schmidt, M., Eds.; Fränkische Geographische Gesellschaft: Erlangen, Germany, 2015.

35. Paloscia, S.; Macelloni, G.; Pampaloni, P.; Santi, E. The contribution of multitemporal SAR data in assessing hydrological parameters. *IEEE Geosci. Remote Sens. Lett.* **2011**, *1*, 201–205.